**Geomechanics and Engineering**, *Vol. 39, No. 3 (2024) 273-282*
https://doi.org/10.12989/gae.2024.39.3.273


# Behavior of seepage in earth dams through complex foundations using three-dimensional finite element method

Truong Q. Nhu[a], Nipawan Kunsuwan[*], Warakorn Mairaing[b], Bunpoat Kunsuwan[c] and Thawatchai Chalermpornchai[d]

*Department of Civil Engineering, Faculty of Engineering at Kamphaeng Saen, Kasetsart University, Kamphaeng Saen, Nakhon Pathom, Thailand*

(*Received April 25, 2024, Revised October 18, 2024, Accepted October 22, 2024*)

**Abstract.** Seepage flow through complex foundations is one of the main factors causing dam failure. To foresee this problem, seepage modeling and analysis are usually performed. This study investigated seepage behavior as affected by complex, foliated, rock foundations in an earth dam. The PLAXIS 3-D LE software was used to analyze seepage problems for steady state flow. The normal high-water level (NHWL) with anisotropic permeability was considered in the models. The anisotropic permeability of foliated rocks was determined according to the angle of inclination. The flow characteristics along the dam axis could be divided into five zones, with three zones for the middle parts (MD1, MD2 and MD3) and one zones for each of the two abutments (LA and RA). The quantities of flow (water transmissibility) upstream to downstream ($Q_X$) on each zone highly depended on the geological structures. Although the average seepage transmissibility values of the residual soil and phyllite were almost equal for every zone. The values in the anticline areas were higher than for the syncline areas, especially for the middle zones. The flow tended to transfer from residual soil into phyllite rock in the anticline area. The transmissibility ratio of anticline to syncline was more than 2 times for both the residual soil and phyllite. The finger drain and river channel attracted substantial flow in the longitudinal ($Q_Y$) and vertical ($Q_Z$) directions. However, the verification of the field piezometric versus the modeling heads showed the possibility of blockage of the finger drain.

**Keywords:** 3-D modeling; complex foundations; earth dam; field monitoring; seepage

## 1. Introduction

One of the main problems in earth dams is seepage failure (Adamo *et al.* 2020), which accounts for 30–50% of total failures in such dams (ICOLD 1994). ICOLD (2020) and Mairaing *et al.* (2023) reported that technical causes of dam failures could arise from spillway capacity, geotechnical issues, hydro-mechanical issues, material ageing, and structural issues. Geotechnical-related cases have been recorded as the major causes of dam failures accounting for more than 58%, as shown in Fig. 1(a). In addition, internal erosion is the greatest contributor of geotechnical failures in earth-fill dams, as shown in Fig. 1(b). Proper seepage modeling and design are required to avoid the adverse effect of internal erosion.

Serious seepage failure with the Teton Dam in 1976 was caused by improper treatment of the dam foundation and hydraulic fracturing at the core trench (U.S. 1977, Wayne 2008). The Wister Dam in Oklahoma, the Stockton Creek Dam in California (Sherard 1986), and the Hyttejuvet Dam in Norway (Ng and Small 1999) were all examples of failure related to internal piping and hydraulic fracturing. Furthermore, seepage problems were reported on the Mun Bon Dam in Thailand (Mairaing and Pintabut 1995).

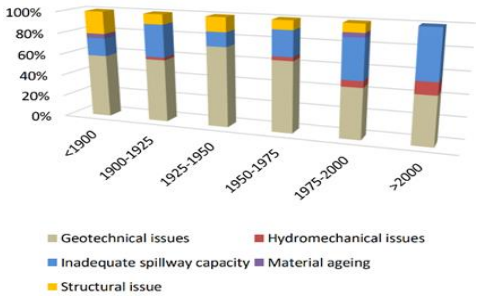


(a) Ratio of failures per cause and failure period

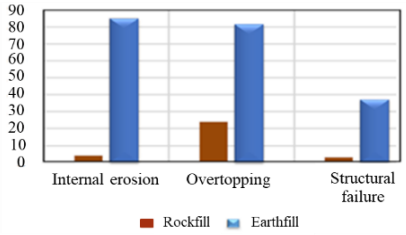


(b) Failure modes on embankment

Fig. 1 Distribution of failure cause and mode on embankment dams (Mairaing *et al.* 2023)

∗Corresponding author, Assistant Professor
E-mail: fengnpw@ku.ac.th
[a]Master student
[b]Associate Professor
[c]Assistant Professor
[d]Research Assistant



ISSN: 2005-307X (Print), 2092-6219 (Online)

This study of a homogenous earth dam on complex foundations can be analyzed using three-dimensional (3-D) seepage modeling. RSIE (2020) reported a case study of a dam constructed in 1972. The dam was damaged in 1995 when water was at NHWL +162.00 m (MSL). The dam had problems of seepage and stability on the downstream slope, where there was local slumping, and a wet area was found in the downstream area. Later, dam piezometers were installed to monitor the dam seepage. In addition, a downstream berm was constructed to stabilize the downstream slope. However, signs of foundation seepage were still observed based on the high pore pressure and wet area.

Generally two-dimensional (2-D) analysis is used for seepage analyses and designing some critical cross sections because of its simplicity (Oya *et al.* 2015). However, in many cases, 2-D models cannot adequately represent flows associated with a complex dam geometry and its foundation conditions. In such complex dam cases, 3-D seepage modeling becomes a necessity (Chen *et al.* 2022). The advantages of 3-D modeling are the interrelated flows in *x*, *y*, and *z*-directions can be analyzed. Then 3-D stability analyses can be followed (Wang *et al.* 2022). However, 3-D model analysis needs substantial more effort and computer resources (Ferdos and Jafarzadeh 2009).

Since the geological structures of the study dam consist of highly foliated phyllite and quartzitic schist, there can be expected anisotropic permeability of materials in different directions (Al-Mansori *et al.* 2020). Furthermore, unsaturated soil properties need to be considered in different dam materials and verification is required of the modeling results by using field monitoring data. Thus, the main objectives of the current study were: 1) to evaluate the behavior of 3-D seepage in the study dam; 2) to compare the seepage transmissibility of different materials and dam sections; and 3) to verify agreement between the hydraulic pressures from the model with the field-measured data.

## 2. Literature review

In recent decades, 2-D finite element method analysis (FEM) has been popular for dam seepage analyses because of its simplicity (Fadaei-Kermani *et al.* 2019, Alzamily and Abed 2022). Haghighi *et al.* (2020) conducted a 2-D seepage analysis of the Doroudzan Dam, Iran using the SEEP/W software. However, the limitations of 2-D modeling become apparent when dealing with complex seepage problems in dams and foundations such as diverse rock forms, faults, layers, and weak structures. Most of the assumptions involved in applying 2-D FEM are insufficient to accurately represent the seepage spatial behavior of the dam and its foundation (Jafarzadeh *et al.* 2009, Sadrekarimi *et al.* 2011).

Many 3-D analyses are performed involving dam abutments or foundations (Strzelecki *et al.* 2018, Rong *et al.* 2019). Rykaart *et al.* (2001) presented examples of 3-D seepage in a soil system using the SVFlux software, by allowing complex geometry to be input from survey data.

The internal erosion of the Gouhou Rockfill Dam associated with the process of water infiltration and hydrological conditions was simulated using 3-D SVFlux software with transient flow (Chen and Zhang 2006). A nonlinear, elastic deformation and an unsteady seepage coupling model were proposed to simulate the seepage and deformation process during modeling by Chen *et al.* (2011). Back analysis based on FEM was applied in a case study to calculate the seepage by considering boundary conditions, groundwater level, permeability parameters, and natural conditions (Ren *et al.* 2016). Seepage from the Kord-Oliya Dam was evaluated using the PLAXIS 3-D software and compared with actual data (Bayat *et al.* 2019).

Several 3-D analyses of earth dams have been performed and checked with field performance (Sjödahl *et al.* 2006, Cho *et al.* 2013, Yun *et al.* 2022). Seepage was modeled using Seep 3-D and an artificial neural network (ANN) model, which showed good agreement with the actual conditions at the Shahid Abbaspour Dam (Shahrbanouzadeh *et al.* 2015). Possible sand boils of the erosion area were observed in the field and analyzed using a 3-D flow model (Schaefer *et al.* 2017). Much research has been performed to verify the seepage distribution of a core wall dam. Guo *et al.* (2022) developed 3-D FEM seepage analysis for an asphaltic and concrete core rockfill dam in Xinjiang, China. The seepage phenomenon in a drainage area was studied by Soualhi and Benmebarek (2022).

After the localized failure of a study dam, much research has been undertaken into the influence of material arching and the hydraulic fracturing zone (Chalermpornchai *et al.* 2021, Kusuwan *et al.* 2023, Mairaing *et al.* 2023). Other studies have evaluated dam seepage and internal erosion based in an expert system (Saejiaw *et al.* 2023). However, some studies have been limited by focusing on 2-D modeling. Therefore, a 3-D model is the next important step to simulate seepage analysis in a complex area for the current dam study.

## 3. Geology of study area

The study dam was a homogenous earth dam with very complex foundations located in the north of Thailand. The dam was designed with a crest elevation of 168.00 m MSL. The maximum flood and NHWL were 166.00 and 162.00 m MSL, respectively. The upstream and downstream dam slopes were 1:3 and 1:2.

The longitudinal profile along the dam axis, a typical dam section and the rock foundation are presented in Figs. 2(a)-2(c). The foliations of phyllite and quartzitic schist are clearly evident from both the bore hole and field observations.

The geological structures were interpreted from regional geology, previous investigation, field borings and tests, and angle of bedding plane of rock coring. The analysis identified the presence of phyllite, chlorite-quartz schist, quartzite, and quartz schist. The dominant structure in the sequence consisted of strongly developed foliation, axial planar to tight to isoclinal folds and dipping shallowly (Singharajwarapan and Berry 1993). The field outcrops showed evidence of an overturned fold or rock bedding of

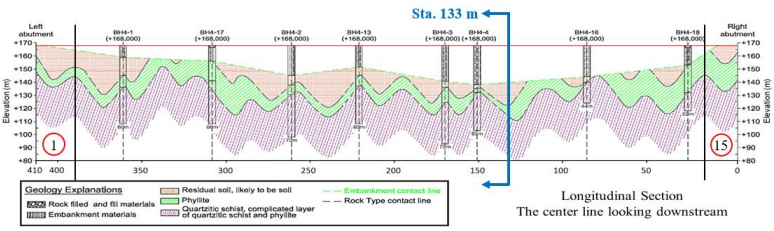


(a) Longitudinal geological profile along dam axis (RSIE 2020)

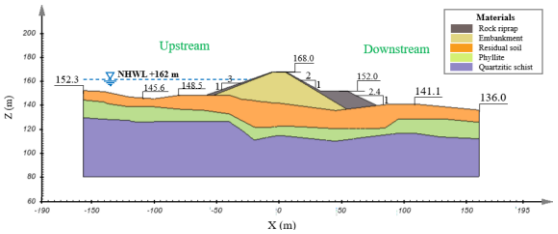


(b) Typical dam at cross-section Sta. 133 m

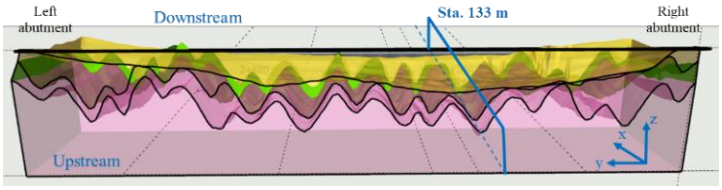


(c) 3-D geological structures (RSIE 2020)

(d) Special folds of rock (Kunsuwan *et al.* 2023)

Fig. 2 Complex foundation in saddle dam

phyllite and quartzitic schist (Kunsuwan *et al.* 2023), as shown in Fig. 2(d).

## 4. Dam incidents

During 1995, the studied dam had a problem with seepage and stability on the downstream slope (RSIE 2020). The reservoir had to retain water above the NHWL from flooding, which caused a high water pressure. Scrap was found with 15 cm settlement and developed into a circular failure on downstream slope. The seepage points, slip plane, and movement from the instability were apparent at the time of failure (Fig. 3(a)).

After that, the dam was repaired and instruments, such as observation wells and piezometers, were installed in the dam body and foundation. However, the wet areas were also found at the downstream toe between folds 4–6, as shown in Fig. 3(b). Then, in 2019, a semi-quantitative risk assessment project was performed to determine the preliminary risk level of the existing dam (GERD 2019). It was concluded that hydraulic fracturing and internal erosion through the foundation were more likely to occur.


(a) Circular failure and sand boil in downstream area

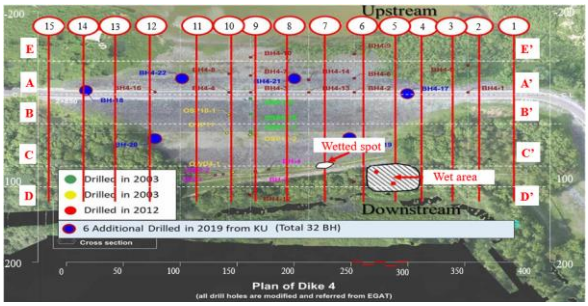


(b) Location of wet areas in downstream area

Fig. 3 Seepage issue in saddle dam (GERD 2019)

## 5. Methodology

### *5.1 Numerical method*

The numerical model was established using the PLAXIS 3-D LE software according to the geological information. The essential inputs included 3-D geometry of the dam embankment, soil and rock foundations, anisotropic permeability, and related boundary conditions, as mentioned in 5.2. The *x*, *y*, and *z*-axes corresponded to the upstream-downstream, dam axis, and vertical directions respectively. Statistical analyses of foliation rock angles were used to verify the anisotropy permeabilities. The angle of inclination every 2 m along the dam axis was used to examine the lateral and vertical permeability. Finally, the analysis results were compared with actual field behavior for verification.

#### *5.1.1 3-D steady-state seepage analysis*

The partial differential equation for flow in the three orthogonal directions is governed by Laplace's Equation of steady-state seepage, following Eq. (1) (Fredlund 2006, PLAXIS LE 2021).

$$\frac{\partial}{\partial x}\left[k_x \frac{\partial h}{\partial x}\right]+\frac{\partial}{\partial y}\left[k_y \frac{\partial h}{\partial y}\right]+\frac{\partial}{\partial z}\left[k_z \frac{\partial h}{\partial z}\right]=0 \qquad (1)$$

where $h$ is the total head and $k_x$, $k_y$, and $k_z$ are the coefficients of permeability in the *x*, *y*, and *z*-directions, for each material, respectively. The *x*, *y*, and *z*-axes were aligned upstream to downstream, right to left abutments and bottom to top, respectively.

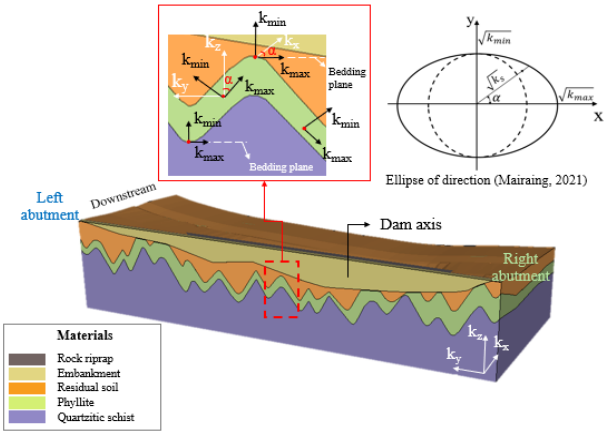


Fig. 4 Ellipse with angle of bedding plane direction

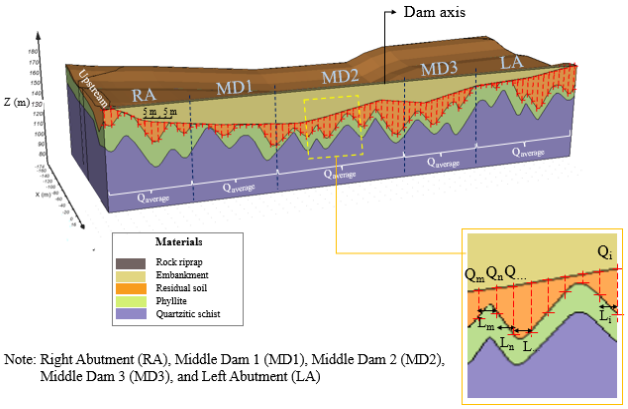


Note: Right Abutment (RA), Middle Dam 1 (MD1), Middle Dam 2 (MD2), Middle Dam 3 (MD3), and Left Abutment (LA)

Fig. 5 Determining zoned flow along dam axis

### 5.1.2 Anisotropy permeabilities

The study case involved anisotropic permeability, where $k_x$, $k_y$, and $k_z$ are different, with $k_x$ considered to be the maximum permeability along the rock bedding plane obtained by field pumping tests. In the other directions, $k_y$ and $k_z$ varied according to the inclination angles of the rock foliation. The calculation involved using the equation of an ellipse for the direction, as shown in Fig. 4 and Eq. (2) (Mairaing 2021):

$$k_a^2 = \frac{k_{\max}^2 . k_{\min}^2}{k_{\max}^2 . \sin_a^2 + k_{\min}^2 . \cos_a^2} \quad (2)$$

where $k_{max}$, $k_{min}$ are permeability along the bedding plane, respectively, and the angle $\alpha$ is the inclination angle between $k_{max}$ and $k_\alpha$, as shown in Fig. 4.

Values for $k_y$ and $k_z$ were calculated every 2 m along the dam axis. The frequency distributions of $k_y$ and $k_z$ were plotted and the mode values of each direction were used as the representative permeability (Liu *et al.* 2017, Shahid *et al.* 2016).

### 5.1.3 Determination of zoned flow

The quantities of flow for each part of the dam were calculated at 5 m intervals along the dam axis. To classify the flow patterns for each material, the average seepage quantity ($Q_{average}$) was considered from 82 flow intervals, as expressed in Eq. (3) and Fig. 5

$$Q_{average} = \frac{\sum_{i=1}^{n}(Q_i \Delta L)}{\sum_{i=1}^{n}(\Delta L)n} = \frac{\sum_{i=1}^{n}(Q_i)}{n} \quad (3)$$

where $Q_{average}$ is the average flow in each zone, $Q_i$ is the average $Q$ for each section for $\Delta L$ = 5 m for each material, and $n$ is the number of $\Delta L$s for each zone.

The best range of flow zones was determined using the coefficient of determination ($R^2$) for flow in the $x$-direction (the major flow direction). Later, these flow zones were used to evaluate the flow behavior for all $x$, $y$, and $z$-directions, with respect to geological variation.

Table 1 Soil and rock properties for 3-D analysis

| Color | Materials | Porosity* | Permeability ($k_x$) (m/s) | Permeability ratio | |
|---|---|---|---|---|---|
| | | | | $k_y/k_x$ | $k_z/k_x$ |
| | Rock riprap | 0.251 | $5.00 \times 10^{-4}$ | 1.000 | 1.000 |
| | Embankment | 0.362 | $6.00 \times 10^{-7}$ | 1.000 | 0.250** |
| | Residual soil | 0.274 | $1.50 \times 10^{-6}$ | 0.021*** | 0.026*** |
| | Phyllite | 0.231 | $3.03 \times 10^{-6}$ | 0.022*** | 0.028*** |
| | Quartzitic schist | 0.173 | $5.25 \times 10^{-7}$ | 0.021*** | 0.023*** |

*Porosity will be equal to the volumetric water content (VWC) at saturated; **values obtained from Sachakamol (1988), Lapkrengkrai (1992); ***presented in anisotropic permeability

## 5.2 Input parameters for 3-D dam seepage modeling

### 5.2.1 Material soil properties

The material permeabilities for the studied dam are summarized in Table 1. The unsaturated materials for the studied dam included the embankment, residual soil, and phyllite. The grain-size distribution curves were obtained from statistical interpretation from the field and laboratory tests, as shown in Fig. 6(a) (RSIE 2020). The soil-water characteristic curve (SWCC) was estimated according to the grain-size distribution and porosity of the soil based on Arya and Paris (1981) method (Arya and Paris 1981, Fredlund *et al.* 2002). Then, the unsaturated permeability function was computed using SWCC by Fredlund, Xing and Huang (1994) estimation (Fredlund *et al.* 1994, PLAXIS LE 2021), as indicated in Fig. 6.

### 5.2.2 Meshing generation and boundary conditions

The geometric parameters ($x$, $y$, $z$ coordinates) of the dam and foundation were measured from the longitudinal section using the AutoCAD software. The geometry of the foliation along longitudinal from the upstream to downstream axis was observed through borehole data, as shown in Figs. 2(a) and 3(b). Then, these data were used to generate the model with adjustment using the Surfer software on a 2×2 m grid. A 3-D FEM numerical model was generated using the PLAXIS 3-D LE software. The $x$-axis ranged from -158 m upstream to 160 m downstream,

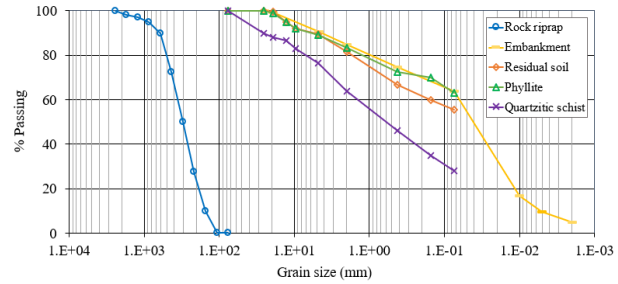


(a) Grain-size distribution curves

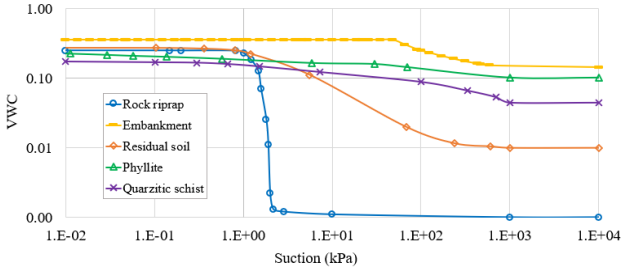


(b) SWCC curves

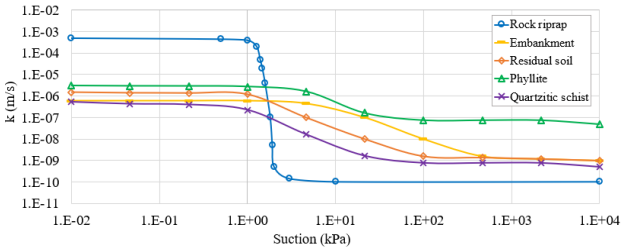


(c) Hydraulic conductivity functions

Fig. 6 Estimating SWCC and hydraulic conductivity functions for material soils

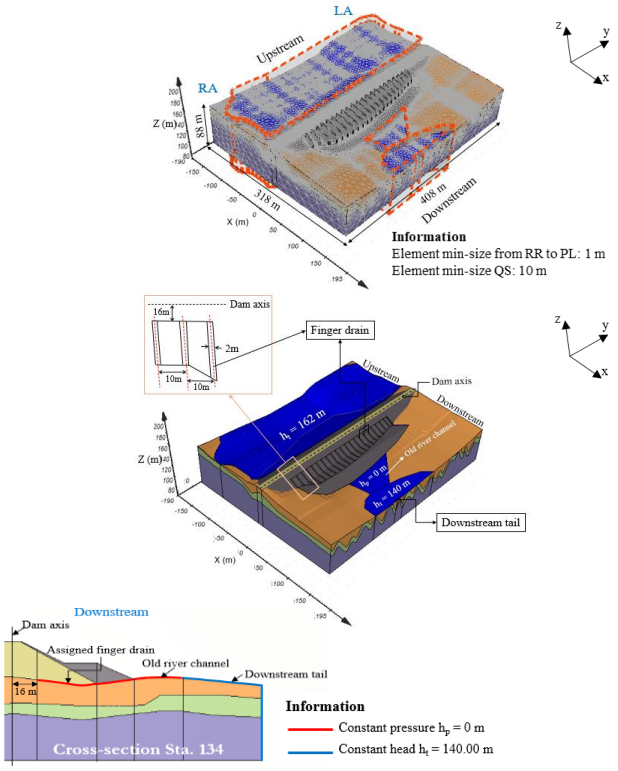


Fig. 7 3-D FE mesh generation and boundary conditions

Table 2 Boundary conditions in FEM

| Region | Boundary condition type | Value (m) |
|---|---|---|
| Upstream | Constant total head at NHWL. | $h_t$ = 162.00 |
| Finger drain | Pressure head at NGL. | $h_p$ = 0.00 |
| Old river channel | Pressure head at NGL. | $h_p$ = 0.00 |
| Downstream tail | Constant total head at NHWL. | $h_t$ =140.00 |

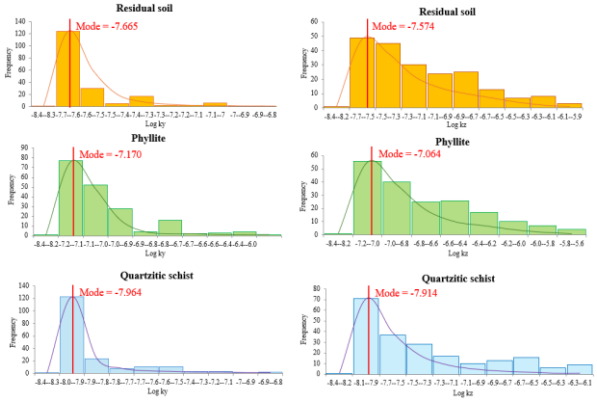


(a) $k_y$ permeabilities (b) $k_z$ permeabilities

Fig. 8 Frequency distribution of anisotropic $k_y$ and $k_z$

covering a distance of 318 m. The *y*-direction from the right to left abutment was 0–408 m. Tetrahedral shape meshes were assigned. In total, 923,830 nodes and 5,218,672 elements were generated for the model. The details of the mesh generation are shown in Fig. 7.

Based on the detailed structure of the dam, a simulation case was considered in NHWL for steady-state seepage analysis. Table 2 shows all the boundary conditions for the complex 3-D FEM profile. Four boundary conditions applied in this model to represent upstream and downstream are also indicated in Fig. 7. The finger drain boundary condition was performed from the tender drawing and dam operation. While other boundary conditions data were observed from field measurements.

## 6. Results and discussions

### *6.1 Anisotropic permeabilities*

As mentioned in Eq. (2) and referenced in Fig. 8, the histograms of the permeability in the *y* and *z*-directions were created to obtain the representative permeability. The values of permeability in each material used in the anisotropy analysis provided a permeability ratio for input to the FEM. The anisotropic properties suggested that the flow aligned parallel to a rock layer had the highest permeability ($k_{max}$), while the flow perpendicular to the rock layer had the lowest permeability ($k_{min}$).

### *6.2 Three-dimensional flow in dam*

#### *6.2.1 Zoned flow along dam axis planes*

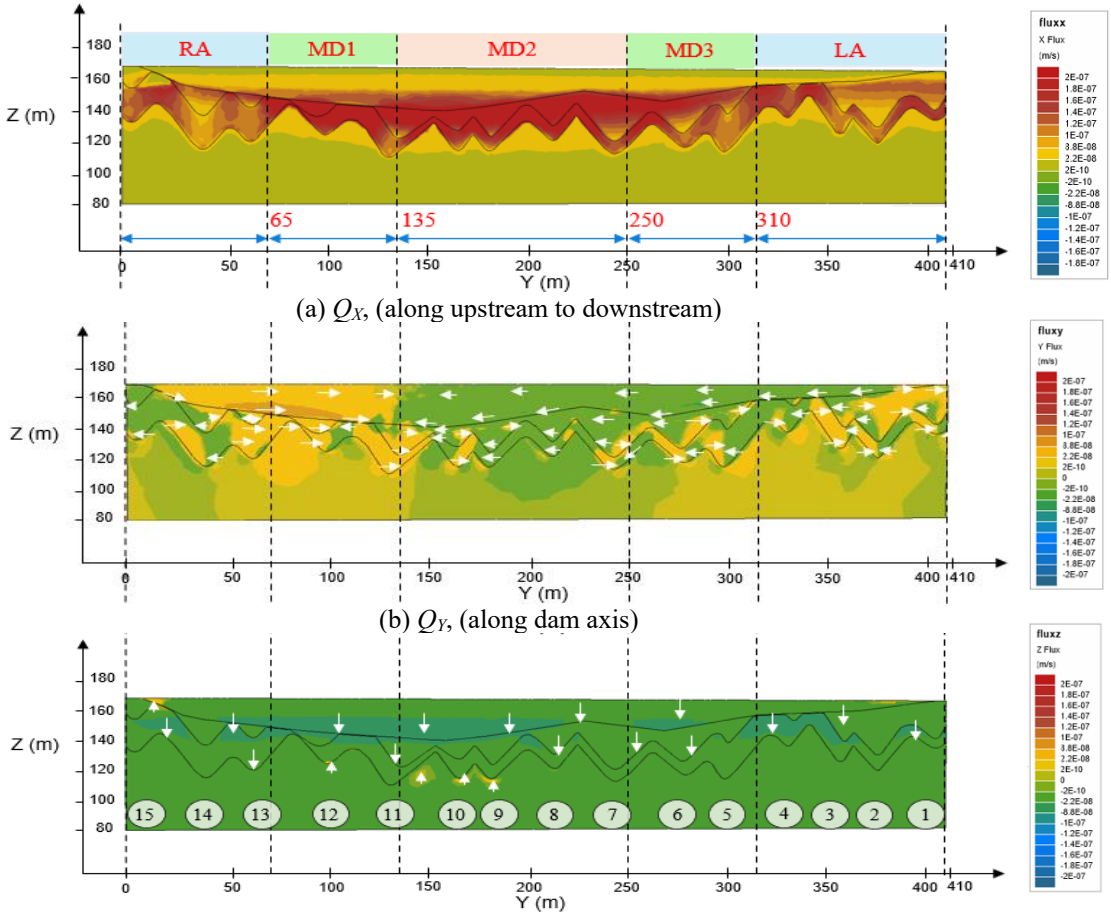


(a) $Q_X$, (along upstream to downstream)

(b) $Q_Y$, (along dam axis)

(c) $Q_Z$, (along vertical axis)

Fig. 9 Zoned flows along *x*, *y*, and *z*-axes at sections on dam axis

The $Q_X$, flow in the upstream to downstream direction constituted the major seepage for the studied dam. The flow was classified according to the method stated in 5.1.3 into five zones namely, RA, MD1, MD2, MD3, and LA. Each zone had a curtain flow characteristic. Fig. 9 indicates the levels of flow on the dam longitudinal section. The total quantities of flow are indicated in Table 3.

The flow along the dam axis in the $Q_X$ direction is presented in Fig. 9(a), showing the intensity of flow in various materials. Residual soil and phyllite had higher flows, especially in MD1 and MD2 compared to the other zones. The flow in the embankment was concentrated in the lower part of the dam. The flow in quartzitic schist was the lowest.

Fig. 9(b) presents the relative lower flow of $Q_Y$ compared to $Q_X$. The directions of flow in the embankment were not affected by the geological structure below but tended to flow from both abutments toward the old river channel. For the anticline area, the water from the residual soil tended to flow into the phyllite layer; however, in the syncline area, no such flow was observed.

Fig. 9(c) illustrates the $Q_Z$ flow downward without any effect of the geological structure.

The relative flow in each material was quantified using the term water transmissibility ($T_R$), as the ability of a material to allow water seepage per unit area. The unit of transmissibility is the flow rate per unit area (in $m^3/s/m^2$ or m/s). Fig. 10 shows the transmissibility ($T_R$) in the $Q_X$ component for each zone. Higher transmissibility was observed in the middle zone (MD1, MD2, and MD3) in Fig. 10(a). The relative $T_R$, as shown in Fig. 10(b), indicated that higher values were on the residual soil and phyllite (40% of the total). On the embankment and quartzitic schist, the $T_R$ values were about 12 and 6%, respectively.

The relative $T_R$ as affected by the geological structures was also studied. Fig. 11 shows the variation in $T_R$ for anticlines and synclines as related to the layer thickness. Anticlines of residual soil and phyllite had greater and wider ranges of $T_R$ compared to synclines, which confirmed that the geological structures had a substantial effect on the flow.

Table 3 Total flow in *x*-direction

| Zoned flow | Total $Q_X$ (m/s) | | | | |
|---|---|---|---|---|---|
| | RA | MD1 | MD2 | MD3 | LA |
| Distance (m) | 0-65 | 65-135 | 135-250 | 250-310 | 310-408 |
| Embankment | $5.50\times10^{-7}$ | $1.15\times10^{-6}$ | $1.84\times10^{-6}$ | $7.35\times10^{-7}$ | $3.58\times10^{-7}$ |
| Residual soil | $1.57\times10^{-6}$ | $3.54\times10^{-6}$ | $5.85\times10^{-6}$ | $1.96\times10^{-6}$ | $2.09\times10^{-6}$ |
| Phyllite | $1.59\times10^{-6}$ | $3.93\times10^{-6}$ | $5.50\times10^{-6}$ | $1.70\times10^{-6}$ | $2.74\times10^{-6}$ |
| Quartzitic schist | $2.34\times10^{-7}$ | $2.96\times10^{-7}$ | $5.54\times10^{-7}$ | $2.73\times10^{-7}$ | $3.22\times10^{-7}$ |

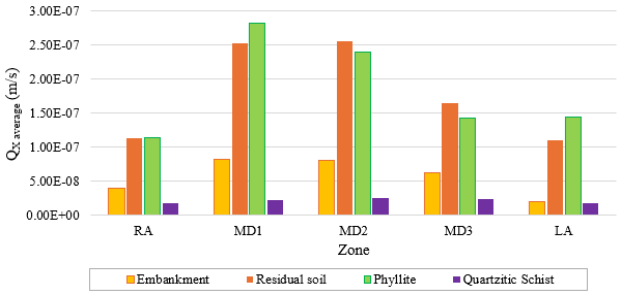


(a) Transmissibility in zoned flow

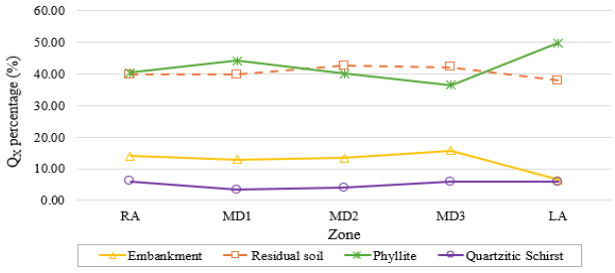


(b) Percentage of transmissibility

Fig. 10 Transmissibility in $Q_X$ along dam axis

Table 4 Ratio of transmissibility between anticline and syncline

| No. | Zone | Soil type | Transmissibility | | $T_{RA}/T_{RS}$ |
|---|---|---|---|---|---|
| | | | Anticline, $T_{RA}$ | Syncline, $T_{RS}$ | |
| 1 | MD1 | Residual soil | $1.20\text{x}10^{-7}x$ | $1.72\text{x}10^{-8}x$ | 6.98 |
| 2 | | Phyllite | $2.17\text{x}10^{-8}x$ | $1.10\text{x}10^{-8}x$ | 1.97 |
| 3 | MD2 | Residual soil | $2.03\text{x}10^{-8}x$ | $9.68\text{x}10^{-9}x$ | 2.10 |
| 4 | | Phyllite | $2.96\text{x}10^{-8}x$ | $1.56\text{x}10^{-8}x$ | 1.90 |
| 5 | MD3 | Residual soil | $1.62\text{x}10^{-8}x$ | $7.55\text{x}10^{-9}x$ | 2.15 |
| 6 | | Phyllite | $8.14\text{x}10^{-9}x$ | $5.62\text{x}10^{-9}x$ | 1.45 |

Table 4 shows the ratio of $T_R$ for anticlines versus synclines. It was clear that the ratio of $T_{RA}/T_{RS}$ was higher for the residual soil than the phyllite.

### *6.2.2 Effect of downstream boundary conditions*

$Q_Y$ and $Q_Z$ on some specific sections had major characteristic flows, as indicated in Fig. 12. For the finger drain section (34 m downstream of the dam axis) and the old river channel (80 m downstream of the dam axis), the boundary conditions were assigned as $h_p$ = 0 m, assuming perfect drainage conditions.

In Fig. 12(a) and $Q_Y$ in the finger drain section, embankment flows were dependent on the foundation geometry and gravity. In the residual soil and phyllite, $Q_Y$ tended to flow into the finger drains. On the river channel, $Q_Y$ also flowed into the river channel area.

In Fig. 12(b), $Q_Z$ in the finger drain section flowed downward from the embankment and upward from the residual soil to the finger drain area in the original ground surface. For the river channel section, the flow was upward to the river channel boundary.

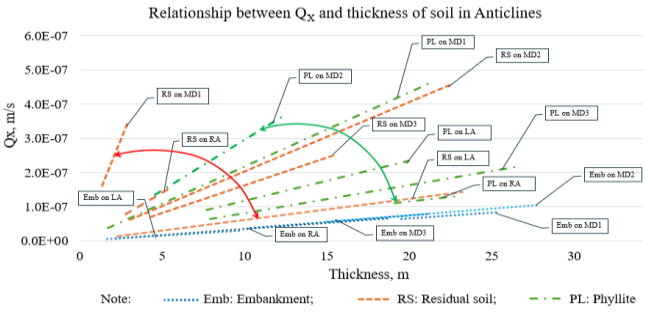


(a) Anticlines

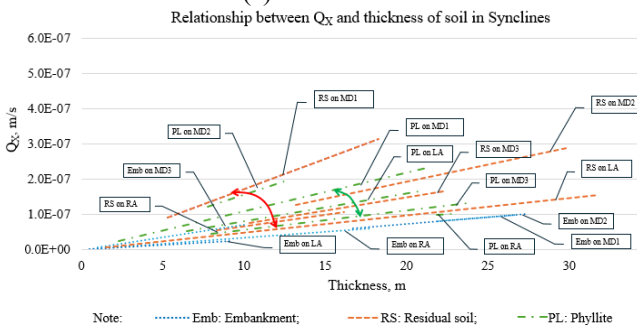


(b) Synclines

Fig. 11 Correlation between $Q_X$ and soil layer thickness along dam axis

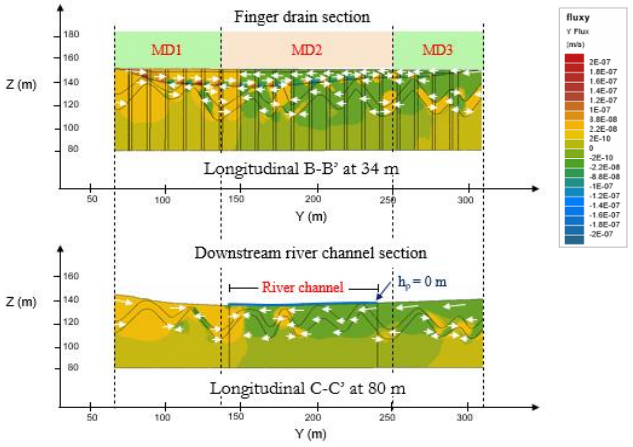


(a) Flow vector of $Q_Y$

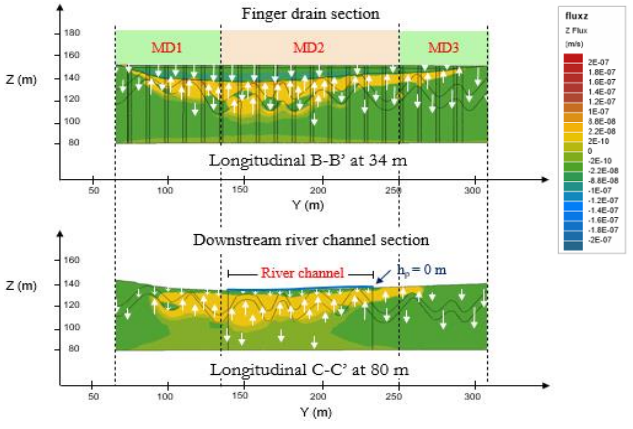


(b) Flow vector of $Q_Z$

Fig. 12 Effect of finger drain and river channel longitudinally

Table 5 Comparison between piezometric head (m MSL) from field monitoring for steady-state FEM in NHWL at 162.00 m (2003 to present)

| No. | Piezometer | Location | | | | | Monitoring head (m) | FEM head (m) | Difference (m) |
|---|---|---|---|---|---|---|---|---|---|
| | | Layer | Zone | x (m) | y (m) | z (m) | | | |
| 1 | OSP8 | Residual soil | Dam center | -5.00 | 174.00 | 134.40 | 159.00 | 146.54 | 12.46 |
| 2 | OSP10 | Residual soil | Dam center | 4.80 | 174.00 | 137.80 | 157.00 | 145.59 | 11.41 |
| 3 | OSP11/1 | Phyllite | Downstream toe | 34.00 | 174.00 | 122.20 | 146.50 | 142.70 | 3.80 |
| 4 | OSP11/2 | Residual soil | Downstream toe | 44.00 | 174.00 | 130.20 | 149.00 | 140.35 | 8.65 |
| 5 | OSP11/3 | Phyllite | Downstream tail | 83.80 | 174.00 | 128.20 | 140.30 | 139.94 | 0.36 |
| 6 | BH 4/3 | Residual soil | Upstream | -30.00 | 174.00 | 140.20 | 157.00 | 155.68 | 1.32 |

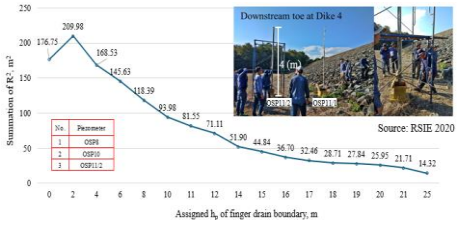


(a) Sum square error ($R^2$) of different heads

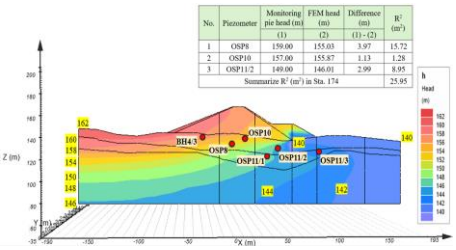


(b) Piezometric heads at cross-section Sta. 174

Fig. 13 Effectiveness of finger drain with assigned downstream boundary condition $h_p$ = 20 m

### *6.3 Comparison of total heads from FEM and actual field monitoring*

The total heads from modeling were compared with the actual field monitoring data, with the verification based on the actual total head observed from piezometer readings.

#### *6.3.1 Saddle dam monitoring system*

The monitoring system for the studied dam was installed after the first repair works. Data were available from 2003 to the present including eight electric piezometers installed in the dam body and foundations for long-term monitoring. The comparison was made on dam cross section at y = 174 m, where the data from six piezometer data were available.

The comparisons are provided in Table 5 and the locations of the instruments are indicated in Fig. 13(b). The head differences were very large for the upstream toward the downstream finger drain. The observed total heads for OSP8, OSP10, and OSP 11/2 were higher than the analysis heads. The high piezometer heads for OSP 11/2 when the head was raised over the elevation for the downstream berm to about 4 m is shown in Fig. 13(a). The head differences reflected several types of behavior in the field such as blockage of the finger drain and hydraulic fracturing of the foundation soil and rock (Chalermpornchai *et al.* 2021, Kunsuwan *et al.* 2023, Mairaing *et al.* 2023, Saejiaw et *al.* 2023).

The study of possible finger drain blockages was done by varying the boundary condition $h_p > 0$ m to match the observation data.

#### *6.3.2 Efficiency of finger drain and downstream boundary condition*

Different boundary pressure heads ($h_p$ = 2, 4, 6, 8, 10, 12, 14, 15, 16, 17, 18, 19, 20, 21, 25 m) were used for the finger drain area based on the assumption that the finger drain could not properly drain the downstream pressure.

Then, the sum square of the different heads ($R^2$) was analyzed and the results are shown in Fig. 13(a). $R^2$ gradually decreased to rather stable values when $h_p$ on the finger drain was higher than 16 m. This value seemed to match with the pressure head observed at OSP 11/2, as shown in Fig. 13(a).

## 7. Conclusions

The study focused on the seepage behavior of an earth dam with complex foundations. The main conclusions from the current study were:

- The majority of flow was in the *x*-axis ($Q_X$) which was concentrated in the residual soil and phyllite rock (80% of total flow in *x*-axis), while flows on the dam embankment and quartzitic schist were 8–16% and 4–6%, respectively, depending on the zone.
- The high transmissibility of $Q_X$ for the residual soil and phyllite were mainly concentrated in anticline compared to syncline areas. The ratio of transmissibility of anticline to syncline ($T_{RA}/T_{RS}$) were 6.98, 2.10, and 2.15 for the residual soil and 1.97, 1.90, and 1.45 for phyllite at MD1, MD2, and MD3, respectively.
- The model of $Q_Y$ and $Q_Z$ indicated major flow patterns into the finger drain and river channel, as specified based on the boundary conditions. For the middle zones (MD1–MD3), the $Q_Y$ flow was into the finger drain and river channel. While $Q_Z$ indicated the vertical flows into finger drain and river channel also.
- Verification of the modelled heads based on the observed piezometric heads indicated that there might be blockages in the downstream drainage system. The blockage creates

the pressure head in the finger drain exceed 16 m as comparing to 0 m for well drain condition.

• The anisotropic permeability of foliated rocks was determined according to the angle of inclination. The modes from the lognormal distributions of $k_y$ and $k_z$ were analyzed. The permeability ratios of $k_y/k_x$ and $k_z/k_x$ were 0.021–0.022 and 0.023–0.028, respectively, for various materials.

## Acknowledgments

This research is funded by Kasetsart University through the Graduate School Fellowship Program and the Department of Civil Engineering, Faculty of Engineering at Kamphaeng Saen, Kasetsart University, Kamphaeng Saen campus, Thailand.

## References

Adamo, N., Al-Ansari, N., Sissakian, V., Laue, J. and Knutsson, S. (2020), "Dam safety problems related to seepage", *J. Earth Sci. Geotech. Eng.*, **10**, 191-239.

Al-Mansori, N., Alfatlawi, T., Othman, N. and Al-Zubaidi, L. (2020), "Numerical analysis of seepage in earth-fill dams", *Civ. Eng. J.*, **6**, 1336-1348. https://doi.org/10.28991/cej-2020-03091552.

Alzamily, Z.N. and Abed, B.S. (2022), "Experimental and theoretical investigations of seepage reduction through zoned earth dam material with special core", *Mater. Today Proc.*, **61**(551), 998-1005. https://doi.org/10.1016/j.matpr.2021.10.283.

Arya, L.M. and Paris, J.F. (1981), "A physicoempirical model to predict the soil moisture characteristic from particle-size distribution and bulk density data", *Soil Sci. Soc. Am. J.*, **45**(6), 1023-1030. https://doi.org/10.2136/sssaj1981.03615995004500060004x.

Bayat, M., Eslamian, S., Shams, G. and Hajiannia, A. (2019), "The 3D analysis and estimation of transient seepage in earth dams through PLAXIS 3D software: neural network", *Environ. Earth Sci.*, **78**(18). https://doi.org/10.1007/s12665-019-8405-y.

Chalermpornchai, T., Kunsuwan, B. and Mairaing, W. (2021), "Simulation of rock crack and permeability in dam foundation during hydraulic fracturing", *Int. J. Geomate*, **21**(86), 55-62. https://doi.org/10.21660/2021.86.j2276.

Chen, Q. and Zhang, L. (2006), "Three-dimensional analysis of water infiltration into the Gouhou Rockfill Dam using saturated–unsaturated seepage theory", *Can. Geotech. J.*, **43**, 449-461.

Chen, Y., Hu, R., Lu, W., Li, D. and Zhou, C. (2011), "Modeling coupled processes of non-steady seepage flow and non-linear deformation for a concrete-faced rockfill dam", *Comput. Struct.*, **89**, 1333-1351.

Chen, Y.F., Yuan, J., Wang, G., Xu, J., Hu, R. and Yang, Z. (2022), "Evaluation of groundwater flow through a high rockfill dam foundation in karst area in response to reservoir impoundment", *Int. J. Rock Mech. Min. Sci.*, **160**(2). https://doi.org/10.1016/j.ijrmms.2022.105268.

Cho, I.K., Ha, I.S., Kim, K.S., Ahn, H.Y., Lee, S. and Kang, H.J. (2013), "3D effects on 2D resistivity monitoring in earth-fill dams", *Near Surf. Geophys.*, **12**(1), 73-81. https://doi.org/10.3997/1873-0604.2013065.

Fadaei-Kermani, E., Shojaee, S., Memarzadeh, R. and Barani, G.A. (2019), "Numerical simulation of seepage problem in porous media", *Appl. Water Sci.*, **9**(79). https://doi.org/10.1007/s13201-019-0965-1.

Ferdos, F. and Jafarzadeh, F. (2009), "Establishing long term seepage behavior of zoned embankment dams with three-dimensional seepage analysis", *Proceedings of the 2nd International Conference on Long Term Behaviour of Dams*, Graz, Austria, October.

Fredlund, D.G. (2006), "Unsaturated soil mechanics in engineering practice", *J. Geotech. Geoenviron. Eng.*, **132**(2).

Fredlund, M.D., Wilson, G.W. and Fredlund, D.G. (2002), "Use of the grain-size distribution for estimation of the soil-water characteristic curve", *Can. Geotech. J.*, **39**(5), 1103-1117. https://doi:10.1139/t02-049.

Fredlund, D.G., Xing, A. and Huang, S. (1994), "Predicting the permeability function for unsaturated soils using the soil-water characteristic curve", *Can. Geotech. J.*, **31**(4).

GERD. (2019), "Semi-Quantitative risk assessment on stability of Saddle Dikes of Sirikit Dam", Final Report; Geotechnical Engineering Research and Development Center (GERD), Electricity Generating Authority, Uttaradit, Thailand.

Guo, D.H., Sun, Y. and Gu, X.B. (2022), "Numerical simulation of a 3D seepage field of an asphaltic and concrete core rockfill dam in an arid area", *Geofluids*. https://doi.org/10.1155/2022/7650527.

Haghighi, A.T., Tuomela, A. and Hekmatzadeh, A.A. (2020), "Assessing the efficiency of seepage control measures in earthfill dams", *Geotech. Geol. Eng.*, **38**(5), 5667-5680. https://doi.org/10.1007/s10706-020-01371-w.

ICOLD. (1994), "Embankment Dams – Granular Filters And Drains", International Commission on Large Dam, Haussmann, Paris.

ICOLD. (2020), General Synthesis, World Register of Dams; World Register of Dams, Haussmann, Paris. https://www.icold-cigb.org/GB/world_register/general_synthesis.asp.

Jafarzadeh, F., Ferdos, F. and Soleimanbeigi, A. (2009), "Comparison between two and three dimensional seepage analysis of rock-fill dams constructed in Narrow Valleys a case study", *Commission Internationale Des Grands Barrages*, Brasilia, Brazil, May.

Kunsuwan, B., Chalermpornchai, T., Mairaing, W. and Thepjanthra, W. (2023), "Asesement of hydraulic fracturing in earth dams on complex foundations", *J. Disaster Res.,* **18**, 270-279. https://doi.org/10.20965/jdr.2023.p0270.

Lapkrengkrai, S. (1992), "Vertical and horizontal permeability of compacted soil", Master Thesis, Kasetsart University, Nakhon Pathom.

Liu, L.L., Cheng, Y.M., Jiang, S.H., Zhang, S.H., Wang, X.M. and Wu, Z.H. (2017), "Effects of spatial autocorrelation structure of permeability on seepage through an embankment on a soil foundation", *Comput. Geotech.*, **87**, 62-75. https://doi.org/10.1016/j.compgeo.2017.02.007.

Mairaing, W. (2021), "Introduction and general concepts for dam design", Designs of Earth and Rockfilled Dam Lectures, Department of Civil Engineering, Kasetsart University, Nakhon Pathom, Thailand.

Mairaing, W. and Pintabut, W. (1995), "Seepage analysis of Mun Bon Dam by finite element method", *KU Eng. J.*, **9**(27), 131-151.

Mairaing, W., Thepjunthra, W. and Chalermpornchai, T. (2023), "Hydraulic fracturing in earth dam monitoring by dam instruments", *Proceeding of the 21st Southeast Asian Geotechnical* Conference *and 4th AGSSEA Conference (SEAGC-AGSSEA 2023)*, Bangkok, Thailand, October.

Ng, A.K.L. and Small, J.C. (1999), "A case study of hydraulic fracturing using finite element methods", *Can. Geotech. J.*, **36**(5), 861-875. https://doi.org/10.1139/t99-049.

Oya, A., Bui, H.H., Hiraoka, N., Fujimoto, M. and Fukagawa, R. (2015), "Seepage flow stability analysis of the riverbank of

Saigon river due to river water level fluctuation", *Int. J. Geomate*, **8**(15), 1212-1217.

PLAXIS LE. (2021), *PLAXIS LE Groundwater 1D/2D/3D Saturated/Unsaturated Finite Element Groundwater Seepage Modeling*, The Bentley Systems Team, Amsterdam, Netherlands.

Ren, J., Shen, Z.Z., Yang, J. and Yu, C.Z. (2016), "Back analysis of the 3-D seepage problem and its engineering applications", *Environ. Earth Sci.*, **75**(2). https://doi.org/ 10.1007/s12665-015-4837-1.

Rong, Y., Zhang, T., Peng, L. and Feng, P. (2019), "Three-Dimensional numerical simulation of dam discharge and flood routing in Wudu reservoir", *Water*, **11**(10). https://doi.org/10.3390/w11102157.

RSIE. (2020), "Preliminary Design for Strengthening of Dike 4, Sirikit Dam", Research Report; Research Center for Sustainable Infrastructure Engineering (RSIE), Electricity Generating Authority, Uttaradit, Thailand.

Rykaart, M., Fredlund, M. and Stianson, J. (2001), "Solving tailings impoundment water balance problems with 3-D seepage software", *Geotech. News*, **35**(7), 50-59.

Sachakamol, P. (1988), "Permeability in soil compaction to construction management", Master Thesis, Kasetsart University, Nakhon Pathom.

Sadrekarimi, J., Kiyani, M., Fakhri, B., Vahdatirad, B.J. and Barari, A. (2011), "Seepage analysis of Upper Gotvand Dam concerning gypsum karstification (2D and 3D approaches)", *Front. Struct. Civ. Eng.*, **5**(1), 71-78. https://doi.org/10.1007/s11709-010-0083-5.

Saejiaw, W., Kunsuwan, B., Mairiang, W., Chalermpornchai, C. and Thongthamehart, C. (2023), "Evaluation of hydraulic fracturing phenomena in earth dam", *J. Eng. Innov.*, **16**(1).

Schaefer, J.A., O'Leary, T.M. and Robbins B.A. (2017), "Assessing the implications of sand boils for backward erosion piping risk", *Proceedings of the Conference of Geo-Risk 2017*, Denver, Colorado, June.

Shahid, R.M., Moshrefy-far, M.R. and Rahimi, N. (2016), "Three-dimensional modeling of the permeability of the rock masses of Khersan 2 dam using geostatistical methods", *Spec. J. Archit. Constr.*, **2**(3), 21-42.

Shahrbanouzadeh, M., Barani, G.A. and Shojaee, S. (2015), "Analysis of flow through dam foundation by FEM and ANN models Case study: Shahid Abbaspour Dam", *Geomech. Eng.*, **9**(4), 465-481. https://doi:10.12989/gae.2015.9.4.465.

Sherard, J.L. (1986), "Hydraulic fracturing in embankment dams", *Int. J. Geotech. Eng.*, **112**(10), 905-927. https://doi.org/10.1061/(ASCE)0733-9410(1986)112:10(905).

Singharajwarapan, S. and Berry, R.F. (1993), "Structural analysis of the accretionary complex in Sirikit Dam area, Uttaradit, northern Thailand", *J. Southeast Asian Earth Sci.*, **8**, 233-245.

Sjödahl, P., Dahlin, T. and Zhou, B. (2006), "2.5D resistivity modeling of embankment dams to assess influence from geometry and material properties", *Geophysics,* **71**(3), 107–114.

Soualhi, M. and Benmebarek, N. (2022), "Experimental and numerical analyzes of parallel drains series performance in earth dams", *Model. Earth Syst. Environ.*, **8**, 1-14.

Strzelecki, T., Uciechowska-Grakowicz, A., Strzelecki, M., Sawicki, E. and Maniecki, Ł. (2018), "Numerical 3D simulations of seepage and the seepage stability of the right-bank dam of the dry flood control reservoir in Racibórz", *Stud. Geotech. Mech.*, **40**(1), 11-20.

U.S. (1977), "Failure of Teton Dam, a report of findings", Fiding Report; U.S. Dept. of the Interior Teton Dam Failure, Washington, United States.

Wang, L., Deng, H., Xu, M., Li, Z., Nie, Y., Huang, Q. and Tang, W. (2022), "Three-Dimensional stability of unsaturated excavation slopes under different seepage conditions: a case study", *Front. Earth Sci.*, **10**. https://doi.org/10.3389/feart.2022.903728.

Wayne, J. (2008), "The Teton Dam Failure - An effective warning and evacuation", *Proceedings of the Association of State Dam Safety Officials 25th Anniversary Conference*, San Diego, California, September.

Yun, T., Butler, K.E. and MacQuarrie, K.T.B. (2022), "Investigation of seepage near the interface between an embankment dam and a concrete structure: monitoring and modeling of seasonal temperature trends", *Can. Geotech. J.*, **60**(4), 453-470. https://doi.org/10.1139/cgj-2022-0169.

*JS*